

## Slurry transport in a pipeline – Comparison of CFD and DEM models

**Dominik KUBICKI<sup>1\*</sup> and Simon LO<sup>1</sup>**

<sup>1</sup>CD-adapco, 200 Sheperds Bush Road, London W6 7NY, UK

\*Corresponding author, E-mail address: dominik.kubicki@cd-adapco.com

### ABSTRACT

In this paper, experimental data of solid distributions in horizontal pipelines were modelled using CFD and Discrete Element Method (DEM). Experimental data were taken from Gilles et al. (2004), Roco et al. (1983) and Hill (1996) for pipe diameter in the range from 51 mm to 103 mm, the average sand particle size from 90  $\mu\text{m}$  to 4400  $\mu\text{m}$  and average solid volume fraction from 0.092 to 0.21. Two CFD models available in STAR-CCM+ for Eulerian multiphase flows were used, the simple solid pressure model that uses the exponential formula for the solid pressure force and more sophisticated model based on the kinetic theory of granular flows that takes into account bulk, collisional, kinetic and frictional viscosities, which result from the presence of solid particles. In both models the turbulent flow was modelled using the standard k- $\epsilon$  model. The drag force acting on the particles was modelled using the Gidaspow formula.

The granular flow model was compared with the DEM implemented in STAR-CCM+. The DEM formulation used in STAR-CCM+ is based on the soft-particle formulation where particles are allowed to develop an overlap. The non-slip Hertz-Mindlin contact model was used to account for particle-particle interactions and the Gidaspow drag formula for liquid-particle interaction. CFD and DEM predictions of solids concentration were compared against experimental data. The comparisons were made in terms of accuracy and computational time.

### NOMENCLATURE

|                      |  |
|----------------------|--|
| $A$                  | constant in solid pressure force equation              |
| $A_j^D$              | linearized drag coefficient                            |
| $c$                  | concentration of solid particles                       |
| $\langle c \rangle$  | average solid concentration                            |
| $C_D$                | drag coefficient                                       |
| $C_L$                | lift coefficient                                       |
| $d$                  | particle diameter                                      |
| $D$                  | pipe diameter  |
| $e$                  | coefficient of restitution                             |
| $F$                  | force  |
| $(F_{\text{int}})_i$ | internal forces  |
| $g$                  | gravitational acceleration                             |
| $g_0$                | radial distribution function                           |
| $I_{2D}$             | second invariant of deviator of the strain rate tensor |
| $M_i$                | interphase momentum transfer                           |
| $p$                  | pressure   |
| $\mathbf{v}$         | velocity   |
| $\mathbf{v}_r$       | relative velocity between phases                       |

|                         |  |
|-------------------------|--|
| $\alpha$                | volume fraction  |
| $\alpha_d$              | volume fraction of dispersed phase                         |
| $\alpha_{d,\text{max}}$ | maximum volume fraction of dispersed phase (packing limit) |
| $\phi$                  | angle of internal friction                                 |
| $\mu$                   | dynamic viscosity  |
| $\mu_p$                 | granular viscosity   |
| $\mu_p^c$               | collisional part of granular viscosity                     |
| $\mu_p^f$               | frictional part of granular viscosity                      |
| $\mu_p^k$               | kinetic part of granular viscosity                         |
| $\mu_{p,\text{max}}^f$  | maximum frictional viscosity                               |
| $\nu$                   | kinematic viscosity  |
| $\nu_c^t$               | turbulent viscosity  |
| $\rho$                  | density  |
| $\sigma_\alpha$         | turbulent Prandtl number                                   |
| $\tau_i$                | stress tensor  |

### INTRODUCTION

Transport of minerals like coal, copper, iron, phosphate and oil sand requires good understanding of slurry behaviour in the pipelines. This paper presents a CFD model of solid distribution in pipelines that gives better insight into the sedimentation process.

In this work two approaches were used, the Eulerian multiphase model and the Discrete Element Method (DEM). The Eulerian multiphase model treats phases as interpenetrating continua. Each phase is characterized by its own physical properties, velocity and temperature. The pressure is shared by the phases and the amount of a given phase in a computational cell is given by the phase volume fraction. The DEM model is based on explicit modelling of the collisions between the particles. This modelling technique uses the Lagrangian approach.

#### Eulerian multiphase model

STAR-CCM+ solves the mass conservation equation for phase  $i$ :

$$\frac{\partial}{\partial t}(\alpha_i \rho_i) + \nabla \cdot (\alpha_i \rho_i \mathbf{v}_i) = 0 \quad (1)$$

and momentum balance takes form:

$$\begin{aligned} \frac{\partial}{\partial t}(\alpha_i \rho_i \mathbf{v}_i) + \nabla \cdot (\alpha_i \rho_i \mathbf{v}_i \mathbf{v}_i) = \\ - \alpha_i \nabla p + \alpha_i \rho_i \mathbf{g} + \nabla \cdot [\alpha_i (\boldsymbol{\tau}_i + \boldsymbol{\tau}_i^t)] + M_i + (F_{\text{int}})_i \end{aligned} \quad (2)$$

where turbulent stresses  $\tau_i^t$  are given by the k- $\epsilon$  model. In this work the standard k- $\epsilon$  model was used to calculate continuous and dispersed phase turbulent stresses that takes into account the extra source terms arise from the presence of the interfacial forces in the momentum balance. The interphase momentum transfer term,  $M_i$ , includes the drag, turbulent dispersion and lift forces.

$F_{\text{int}}$  is the internal force and in this study it includes the solid pressure force that occurs in the particle phase only. Details of these forces are given below.

#### Drag force

In this work, the Gidaspow formula for the drag force was used. It connects the Ergun equation for high solid particle concentration with a modified Stokes law for regions of low and moderate concentrations. The linearized drag coefficient  $A_{ij}^D$  is given by:

$$A_{ij}^D = \begin{cases} \frac{150\alpha_d^2\mu_c + 1.75\alpha_d\rho_c|v_r|}{\alpha_c d^2} & \alpha_d \geq 0.2 \\ \frac{3}{4}C_D \frac{\alpha_d\rho_c}{d} |v_r| \alpha_c^{-1.65} & \alpha_d < 0.2 \end{cases} \quad (3)$$

where  $C_D=0.44$ . The drag force is given by:

$$F_{ij}^D = A_{ij}^D (v_j - v_i) \quad (4)$$

#### Turbulent dispersion force

Ekambara (2009) showed the importance of the turbulent dispersion force in predicting the distribution of solid particles in pipes. The turbulent dispersion force accounts for the interaction between the dispersed particles and the surrounding turbulent eddies. The following formula was used:

$$F_{ij}^{DT} = A_{ij}^D \frac{v_c^t}{\sigma_\alpha} \left( \frac{\nabla \alpha_j}{\alpha_j} - \frac{\nabla \alpha_i}{\alpha_i} \right) \quad (5)$$

where  $\sigma_\alpha$  is the turbulent Prandtl number equal to 1.

#### Lift force

In a non-uniform or swirling flow field the dispersed particles experience a lift force that is perpendicular to the relative velocity. STAR-CCM+ uses a formula from Auton (1988):

$$F_L = C_L \alpha_d \rho_c [v_r \times (\nabla \times v_r)] \quad (6)$$

and the value of the lift coefficient  $C_L$  is 0.1, which is commonly used for small solid particles (Ekambara et al. 2009).

#### Solid pressure force

The presence of solid particles results in an additional solid pressure force that needs to be added to the momentum balance. The solid pressure force accounts for the particle-particle interaction when the solid volume fraction is close to the maximum packing limit. This force appears in the solid phase momentum equation only. In this work an exponential formula was used:

$$(F_{\text{int}})_d = -[e^{A(\alpha_{d,\text{max}} - \alpha_d)}] \nabla(\alpha_d) \quad (7)$$

#### Granular flow model

The granular flow model offers a more accurate representation of the solid particles than the simple solid pressure force model. Two regimes can be distinguished in the granular flow model depending on concentration of the particles.

#### Granular flow model - kinetic regime

In the kinetic regime the volume fraction of particles is lower than the maximum packing limit and the probability of collisions between particles is characterized by the radial distribution function  $g_0$  (Ding 1990)

$$g_0 = \frac{3}{5} \left[ 1 - \left( \frac{\alpha_d}{\alpha_{d,\text{max}}} \right)^{1/3} \right]^{-1} \quad (5)$$

The radial distribution function is used to calculate the granular temperature  $\theta_p$  that determines the effective granular viscosity.

The effective granular viscosity is composed of collisional and kinetic parts.

$$\mu_p = \mu_p^c + \mu_p^k \quad (6)$$

The collisional part is given by:

$$\mu_p^c = \frac{4}{5} \alpha_d^2 \rho_d d g_0 (1+e) \sqrt{\frac{\theta_p}{\pi}} \quad (7)$$

whereas the kinetic part comes from Gidaspow (1994):

$$\mu_p^k = \frac{10\rho_d d \sqrt{\pi\theta_p}}{96(1+e)g_0} \left[ 1 + \frac{4}{5} g_0 \alpha_d (1+e) \right]^2 \quad (8)$$

#### Granular flow model - frictional regime

In the frictional regime the volume fraction of particles is close to the packing limit and the solid pressure force is given by (Schaeffer 1987):

$$p_p^f = \begin{cases} 10^{25} (\alpha_d - \alpha_{d,\text{max}})^{10} & \alpha_d > \alpha_{d,\text{max}} \\ 0 & \alpha_d \leq \alpha_{d,\text{max}} \end{cases} \quad (9)$$

and the effective granular viscosity is given by:

$$\mu_p^f = \begin{cases} \min \left( \frac{p_p^f \sin \phi}{\sqrt{4I_{2D}}}, \mu_{p,\text{max}}^f \right) & \alpha_p > \alpha_{p,\text{max}} \\ 0 & \alpha_p \leq \alpha_{p,\text{max}} \end{cases} \quad (10)$$

where  $\phi$  is the angle of internal friction and  $I_{2D}$  is the second invariant of deviator of the strain rate tensor. Schaeffer (1987) recommend using 25 deg. for the angle of internal friction.

#### DEM model

STAR-CCM+ uses the DEM model based on the soft-particle formulation where an overlap between particles is allowed.

Momentum balance takes form:

$$F_b = F_g + F_u + F_c \quad (11)$$

where  $F_g$  is the gravitational force,  $F_u$  the drag force and  $F_c$  the contact force that includes wall-particle and particle-

particle interactions. The contact forces between particle-particle and particle-wall are modelled using the Hertz-Mindlin model (Di Renzo 2004). In this model the contact force between two particles is decomposed into the normal and tangential components. Both component forces take into account of stiffness and damping.

The interaction between the liquid phase and particles is strong and the two-way coupling with the continuous phase was used in this work. The two-way coupling allows the Lagrangian phase to exchange the momentum with the continuous phase.

## CFD MODEL

The CFD model was constructed using the STAR-CCM+ software. Experiments from Gilles (2004), Roco (1983) and Hill (1996) were simulated. The pipe diameter varied from 51 mm to 103 mm, the particle size was in the range from 90  $\mu\text{m}$  to 4400  $\mu\text{m}$  and the average solid volume fraction from 0.092 to 0.21. A summary of the modelling conditions is given in Table 1.

| case | $\alpha$ | $D$<br>[mm] | $d$<br>[ $\mu\text{m}$ ] | $v$<br>[m/s] | $\rho_p$<br>[ $\text{kg}/\text{m}^3$ ] |
|------|----------|-------------|--------------------------|--------------|--|
| 1    | 0.19     | 103         | 90                       | 3            | 2650                                   |
| 2    | 0.189    | 51.5        | 165                      | 4.17         | 2650                                   |
| 3    | 0.20     | 51.5        | 270                      | 5.4          | 2650                                   |
| 4    | 0.203    | 51.5        | 480                      | 3.41         | 2650                                   |
| 5    | 0.0918   | 51.5        | 165                      | 3.78         | 2650                                   |
| 6    | 0.15     | 53          | 4400                     | 1.75         | 2470                                   |

**Table 1:** Modelling conditions.

All conditions were modelled using the granular flow model. The exponential form of solid pressure was used for conditions 1-5. Due to hardware limitations DEM model was used only for the largest particle (condition 6). For conditions 1-5 the number of particles required in a DEM calculation is in the order of  $1e7$  that makes it computationally expensive hence DEM calculations were not performed for these cases.

CFD simulations were run on a 3D grid with 720k cells shown in Figure 1. It is necessary to use a 3D grid as the gravitational acceleration acts perpendicular to the pipe axis. The grid sensitivity was studied on grids from 720k to 1.5M cells and solution was found to be grid independent at 720k cells. The grid was constructed with 10 prism layers. Since the k- $\epsilon$  model with wall function was used, the first cell in the prism layer was located in the logarithmic region of the boundary layer. The distance from the wall varied from  $y^+=40$  to  $y^+=140$  with average value of 60. Velocity inlet and pressure outlet were used as boundary conditions. Uniform solid concentration was used at the inlet. The length of the pipe was 10m.

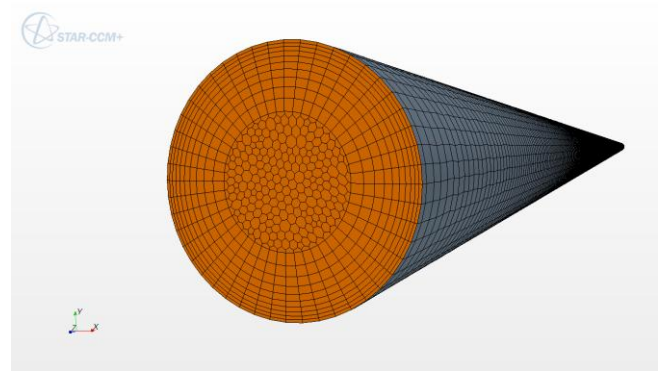


**Figure 1:** Computational grid.

All simulations were run as unsteady in time with the time step of  $1e-3\text{s}$  for the exponential form of solid pressure and the granular flow model and  $1e-5\text{s}$  for DEM.

## CFD RESULTS

Normalized solid concentration vs. normalized pipe height at 9m from the inlet is plotted in Figures 2-6. The solid concentration profiles correspond to the steady state profile that is formed in a long horizontal pipe.

Results for the simulations using the exponential form of solid pressure and the granular flow model are similar in the case of uniform solid concentration (Figure 2) and non-uniform solid concentration (Figure 5). Both models correctly predict the effect of particle size (Figure 3,  $d=165\mu\text{m}$  and Figure 4,  $d=270\mu\text{m}$ ), pipe diameter (Figure 2,  $D=103\text{mm}$  and Figure 3,  $D=51.5\text{mm}$ ) and effect of average solid volume fraction (Figure 5,  $\alpha=0.203$  and Figure 6,  $\alpha=0.0918$ ).

Figures 3 and 6 show that there are some differences between the granular flow model and the exponential form of solid pressure when the solid particles are close to the pipe wall. This difference results from the extrapolation boundary conditions for granular temperature used for the pipe wall. Also the concentration of particles is not measured accurately near the pipe wall and there are not enough experimental points to validate the model in this region. Figure 5 shows the small kink in the measured solid concentration near the pipe wall indicating that the granular flow model may be more accurate in this region.

Computations using the granular flow model were about 25% slower than the solid pressure force model.

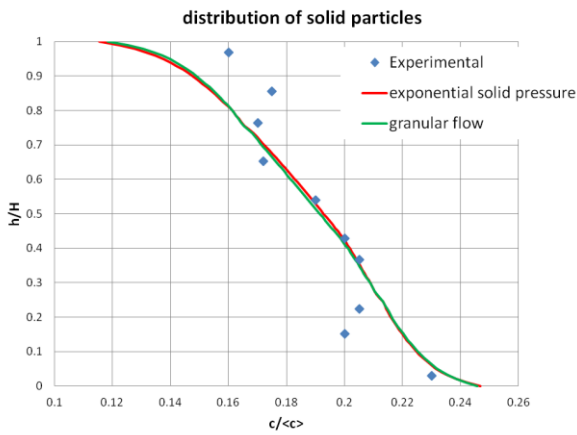


**Figure 2:** Results for case 1 ( $\alpha=0.19$ ,  $D=103\text{mm}$ ,  $d=90\mu\text{m}$ ,  $v=3\text{ m/s}$ ,  $\rho_p=2650\text{kg/m}^3$ )

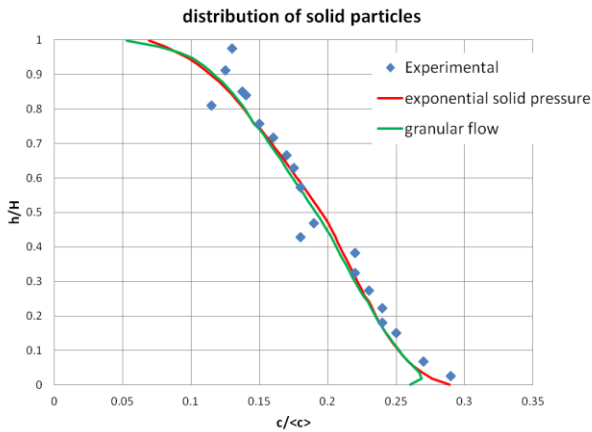


**Figure 3:** Results for case 2 ( $\alpha=0.189$ ,  $D=51.5\text{mm}$ ,  $d=165\mu\text{m}$ ,  $v=4.17\text{ m/s}$ ,  $\rho_p=2650\text{kg/m}^3$ )

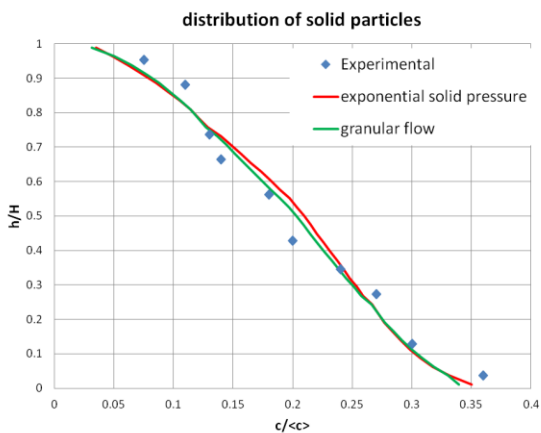


**Figure 4:** Results for case 3 ( $\alpha=0.20$ ,  $D=51.5\text{mm}$ ,  $d=270\mu\text{m}$ ,  $v=5.4\text{ m/s}$ ,  $\rho_p=2650\text{kg/m}^3$ )

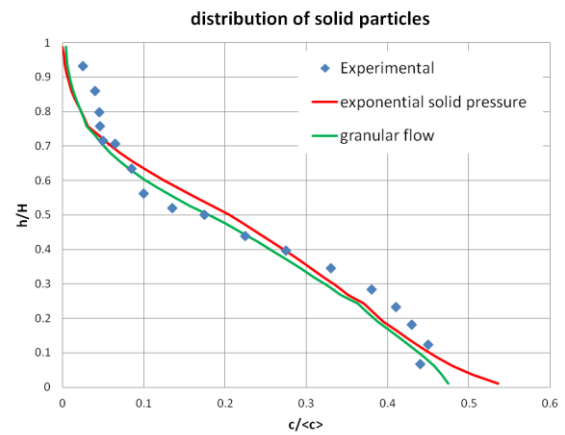


**Figure 5:** Results for case 4 ( $\alpha=0.203$ ,  $D=51.5\text{mm}$ ,  $d=480\mu\text{m}$ ,  $v=3.41\text{ m/s}$ ,  $\rho_p=2650\text{kg/m}^3$ )

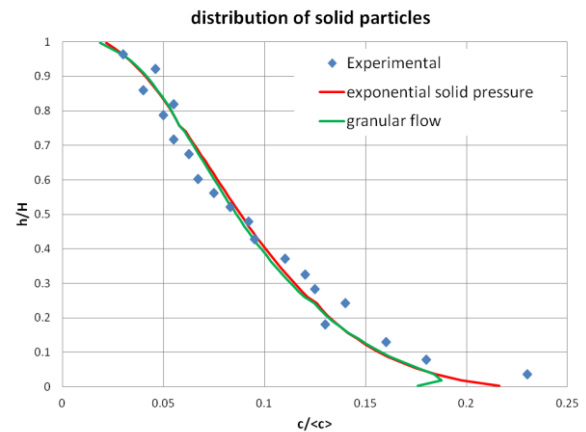


**Figure 6:** Results for case 5 ( $\alpha=0.0918$ ,  $D=51.5\text{mm}$ ,  $d=165\mu\text{m}$ ,  $v=3.78\text{ m/s}$ ,  $\rho_p=2650\text{kg/m}^3$ )

The comparison of velocity and volume fraction profiles in Figures 7-10 shows that both models give almost identical solution. The velocity profiles, shown in Figures 7 and 8, develop in the same way for two models. Also the settling of particles show in Figures 9 and 10 is almost the same for the granular flow model and the exponential solid pressure model.

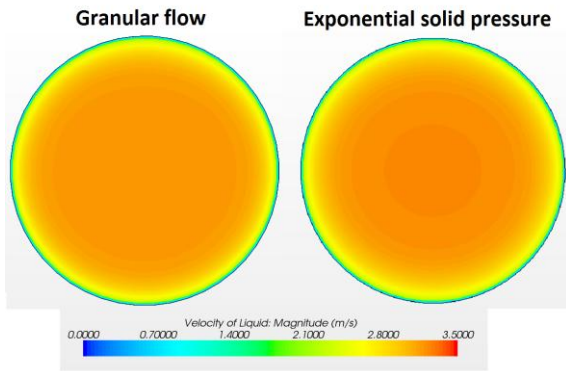


**Figure 7:** Results for case 1 velocity at 1m ( $\alpha=0.19$ ,  $D=103\text{mm}$ ,  $d=90\mu\text{m}$ ,  $v=3\text{ m/s}$ ,  $\rho_p=2650\text{kg/m}^3$ )

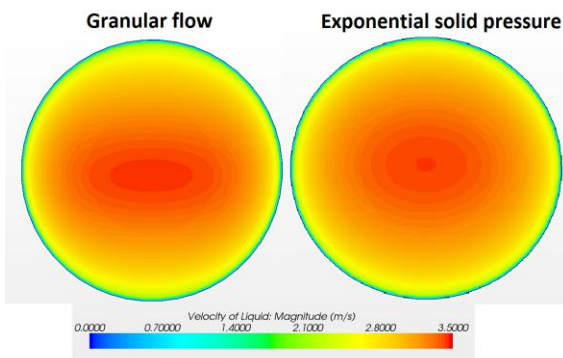


**Figure 8:** Results for case 1 velocity at 5m ( $\alpha=0.19$ ,  $D=103\text{mm}$ ,  $d=90\mu\text{m}$ ,  $v=3\text{ m/s}$ ,  $\rho_p=2650\text{kg/m}^3$ )

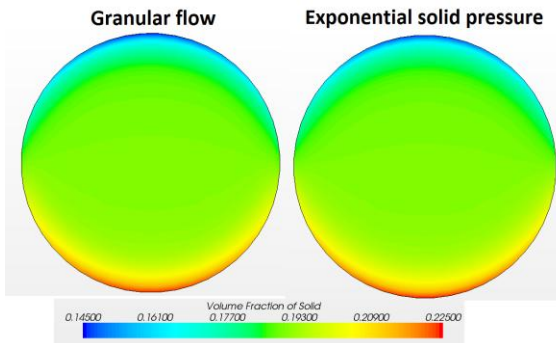


**Figure 9:** Results for case 1 solids at 1m ( $\alpha=0.19$ ,  $D=103\text{mm}$ ,  $d=90\mu\text{m}$ ,  $v=3\text{ m/s}$ ,  $\rho_p=2650\text{kg/m}^3$ )

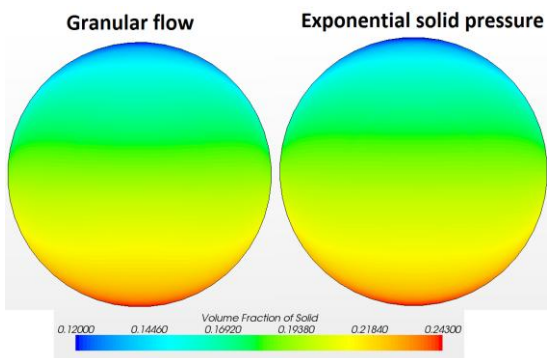


**Figure 10:** Results for case 1 solids at 5m ( $\alpha=0.19$ ,  $D=103\text{mm}$ ,  $d=90\mu\text{m}$ ,  $v=3\text{ m/s}$ ,  $\rho_p=2650\text{kg/m}^3$ )

The DEM simulation was about 7 times slower than the simulations with the granular flow model. Results from the DEM simulation are shown in Figure 11. In this case of large particles (4.4mm in 53 mm pipe) the DEM model is more accurate. There is a small error in the upper part of the pipe cross-section that most probably results from turbulence modelling and the lack of turbulent dispersion effects in this case resulting in a lower particle concentration. There are also some differences near the bottom wall of the pipe. The DEM model predicts that the particle concentration drops to 0.2 near the wall. Experimental data in this region is scattered.

The granular flow model in this case of large particles is less accurate. For this case only, the granular flow simulation was performed without the turbulent dispersion force since it is not important for particles larger than the turbulent eddies. The granular flow model predicts more settling than DEM and experimental data. One possible reason for this is that with the larger particles and smaller pipe-to-particle diameter ratio, the particle-wall contacts create a significant larger void than the usual particle-particle contacts. DEM represents this larger void near the lower pipe wall correctly whereas the granular flow model does not.

Figure 12 shows an instantaneous concentration of particles near the inlet. The steady state profile is formed at about 4-5 diameters from the inlet.

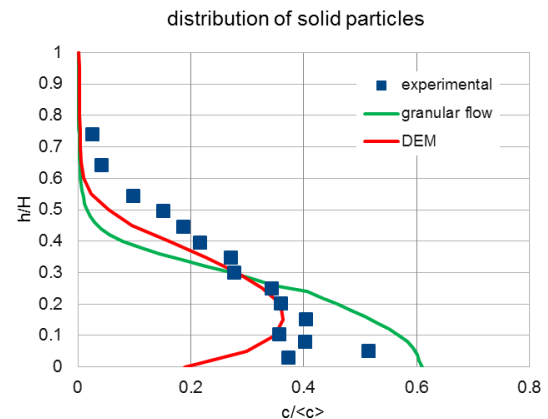


**Figure 11:** Results for case 6 ( $\alpha=0.15$ ,  $D=53\text{mm}$ ,  $d=4400\mu\text{m}$ ,  $v=1.75\text{ m/s}$ ,  $\rho_p=2470\text{kg/m}^3$ )

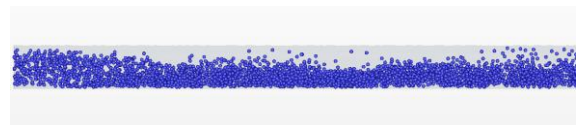


**Figure 12:** Distribution of solid particles for case 6 ( $\alpha=0.15$ ,  $D=53\text{mm}$ ,  $d=4400\mu\text{m}$ ,  $v=1.75\text{ m/s}$ ,  $\rho_p=2470\text{kg/m}^3$ )

## CONCLUSION

The Eulerian Multiphase model implemented in STAR-CCM+ correctly predicted the distribution of solid particles in horizontal pipes for a wide range of particle sizes, pipe diameters and flow rates. The predictions are close to the experimental data for cases when solids are

well distributed (Figure 2) and also when the distribution of solids is poor (Figure 5). When the ratio of pipe diameter to particle diameter is small, close to 10, the accuracy of Eulerian simulations decreases.

Two models for solid pressure implemented in STAR-CCM+, the simple exponential form and the granular flow model give similar results. The granular flow model is more accurate near the pipe wall but it is about 25% slower than the exponential form of solid pressure.

The DEM simulation requires more computational resources and was performed only for one case with large particles. In this case it is more accurate than the Eulerian model. However, the DEM simulation takes about 7 times more computing time than the equivalent Eulerian simulation.

## REFERENCES

- AUTON, T.R., HUNT, J.C.R., and PRUD'HOMME, M. (1988), "The force exerted on a body in inviscid unsteady non-uniform rotational flow", *J. Fluid Mech.*, **197**, 241-257.
- DI RENZO, A., and DI MARIO, F. P., (2004) "Comparison of contact-force models for the simulation of collisions in DEM-based granular flow codes", *Chemical Engineering Science* **59**, 525-541.
- DING, J., and GIDASPOW, G., (1990) "A bubbling fluidisation model using kinetic theory of granular flow." *AIChE Journal*, **36(4)**, 523-538.
- EKAMBARA, K., SANDERS, R.S., NANDAKUMAR, K., and MASLIYAH, J.H. (2009) "Hydrodynamic simulation of horizontal slurry pipeline using ANSYS-CFX". *Ind. Eng. Chem. Res.* **48**, 8159-8171.
- GIDASPOW, D., (1994) "Multiphase Flow and Fluidization - Continuum and Kinetic Theory Descriptions." Academic Press.
- GILLES, R.G., SHOOK, C.A., and XU J. (2004) "Modeling Heterogeneous slurry flow at high velocities" *Can. J. Chem. Engng.* **82**, 1060-1065
- HILL, K.B., (1996) "Pipeline flow of coarse particles in fluids with yield stress" *PhD Thesis*, University of Saskatchewan, Canada
- ROCO, M., and SHOOK, C.A. (1983) "Modeling of slurry flow: the effect of particle size" *Can. J. Chem. Engng.* **61**, 494-503.
- SCHAEFER, G., (1987) "Instability in the evolution equations describing incompressible granular flow." *J. Diff. Equ.*, **66**, 19-50.